Effect of electric field on water free energy in graphene nanochannel

Cite as: J. Appl. Phys. **132**, 015104 (2022); https://doi.org/10.1063/5.0080876
Submitted: 04 December 2021 • Accepted: 22 June 2022 • Published Online: 06 July 2022

Dezhao Huang, Shiwen Wu, Guoping Xiong, et al.

Journal of Applied Physics ARTICLE scitation.org/journal/jap

Effect of electric field on water free energy in graphene nanochannel

Cite as: J. Appl. Phys. **132**, 015104 (2022); doi: 10.1063/5.0080876
Submitted: 4 December 2021 · Accepted: 22 June 2022 ·
Published Online: 6 July 2022

Dezhao Huang,[1] Shiwen Wu,[2] Guoping Xiong,[2,a)] and Tengfei Luo[1,3,a)]

AFFILIATIONS

[1]Department of Aerospace and Mechanical Engineering, University of Notre Dame, Notre Dame, Indiana 46556, USA
[2]Department of Mechanical Engineering, The University of Texas at Dallas, Richardson, Texas 75080, USA
[3]Department of Chemical and Biomolecular Engineering, University of Notre Dame, Notre Dame, Indiana 46556, USA

[a)]**Authors to whom correspondence should be addressed:** Guoping.Xiong@utdallas.edu and tluo@nd.edu

ABSTRACT

Graphene nanochannels and nanostructures have been of great interest to applications like nanofluidics and solar-thermal evaporation since nanoconfinement can lead to altered liquid properties. In this article, we employ molecular dynamics simulations combined with the free energy perturbation method to study the influence of external electric fields on the free energy of water molecules in graphene nanochannels. We observe a decrease in the water free energy difference ($\Delta G_{1-0} = G_0 - G_1$, where 0 is the reference vacuum state and 1 is the solvated state) with the increasing electric field, suggesting that the application of an electric field may reduce the thermal energy needed to evaporate water from graphene nanochannels. Our analysis reveals that the reduction in free energy difference is related to more aligned water molecules along the electric field direction in the nanochannels, which leads to a decrease in the water inter-molecular potential energy and, thus, reduces the free energy difference.

INTRODUCTION

Understanding the behavior and properties of water confined in nanochannels is of particular importance for a wide range of applications, ranging from nanofluidics[1,2] to renewable energy conversion.[3–8] Studies have shown that some thermodynamic properties of water confined in nanochannels can be different from those of bulk water.[9–12] For example, Knight *et al.*[9] have experimentally demonstrated that nanoconfinement could lead to a decrease in the surface tension of water by 30%. Santiburcio *et al.*[10] conducted *ab initio* simulations on nanoconfined water and found that nanoconfinement enhanced water self-dissociation. Garofalini *et al.*[11] found that nanoconfined water exhibited anomalously high thermal expansion from molecular dynamics (MD) simulations, and Neek-Amal *et al.*[12] also conducted MD simulations to find the shear viscosity to be greatly enhanced in nanoscale capillaries. In a more recent study, Zhao *et al.*[7] inferred from their experiment that the latent heat of the water in a nanostructured molecular hydrogel mesh could be reduced by 60%; however, the mechanism is under debate and whether the observation was related to the nanoconfinement effect remains unclear.

The effects of nanoconfinement in liquid transport properties have also been studied. Giovambattista *et al.* found that the effective hydrophobicity of the surface of a nanochannel decreases as temperature decreases[13] and observed that the confined water remains in the liquid state while the bulk water cavitates at the same pressure.[14] MD simulations have predicted that changing the distance between two parallel surfaces can induce the freezing and melting of a monolayer and a bilayer of liquid water.[15,16] Gao *et al.*[17] showed that the interfacial commensurability would influence the thin liquid film's diffusion and rheological characteristics. Leoni *et al.*[18] compared three different liquids in a graphene slit pore and found three different free-energy minima mechanisms. Figueras *et al.*[19] have shown that water permeation could be substantially reduced for field intensities of 2–3 V/nm, and no water permeation was observed under the perpendicular 4 V/nm fields.

On top of nanoconfinement, several molecular simulation studies have found that external interferences from electric or magnetic fields can also impact the thermodynamic properties of nanoconfined water.[20–22] For instance, Srivastava *et al.*[23] examined the influence of an external electric field on the vapor–liquid coexistence curve using MD simulations and observed that the critical temperature of confined water decreased with the increase in

electric field strength. Maerzke *et al.*[24] conducted Gibbs ensemble Monte Carlo simulations to investigate the influence of electric field on water/vapor equilibria and found that water molecules tended to orientationally order themselves in the electric field. Yeh *et al.*[25] also conducted MD simulations with a high electric field imposed on water and observed that the dielectric constant of water decreased with the increasing electric field.

Carbon materials such as carbon black,[5] graphene derivatives (e.g., graphene oxides[26]), and carbon nanotubes have acted as wall materials of nano-sized channels in nanofluidics and energy applications.[2,27,28] In solar thermal applications,[8,26,29] carbon materials also function as ideal light-absorbers. Recently, Xiong *et al.*[30–32] have designed a series of graphene nanopetal solar evaporators with high vapor generation performance, and in particular, they have demonstrated that a hierarchical, integrated graphene nanoarchitecture can achieve highly efficient solar-thermal energy conversion for water evaporation.[30] Besides providing graphene nanochannels for water transport in these structures, it is reported that the plasmonic effect could potentially lead to strong localized electric fields in the vicinity of graphene nanopetals.[33] The question is: whether nanoconfined graphene channels combined with strong electric fields can potentially lead to changes in water thermodynamic properties? The answer to this question would help guide the rational design of nanomaterials for different applications such as solar-thermal water evaporation.

In this study, we carry out MD simulations combined with the free energy perturbation method to calculate the free energy of water in a graphene nanochannel in the presence of an external electric field. Different electric field strengths (0.1–0.5 V/Å) are studied to examine their impacts on the nanoconfined water. It is found that the nanoconfined environment and the electric field can both result in a decrease in water free energy difference (defined as $\Delta G_{1-0} = G_0 - G_1$, where 0 is the reference vacuum state and 1 is the solvated state), which could potentially make water molecules easier to evaporate. It is also found that the strong electric field forces water dipoles to align with the electric field direction, which lowers the potential energy among water molecules and, thus, leads to decreased free energy difference.

METHODS AND SIMULATION MODEL

The simulation model consists of 900 water molecules confined between two graphene layers as shown in Fig. 1(a). To calculate the free energy, one water molecule is extracted from the channel [Fig. 1(b)].

Graphene layers with the dimensions of ~20 Å(x) × 50 Å(y) are used as the channel wall, and the width of the channel is ~30 Å. Periodic boundary conditions are applied in the x- and y-directions. Water molecules are simulated based on the TIP3P-Ew model,[34] which can reproduce water structures well.[35–37] Two O–H bonds and the H–O–H angle are held rigid. The graphene layers are modeled using the Adaptive Intermolecular Reactive Empirical Bond Order potential (AIREBO) potential, which has been used for interfacial simulations involving graphene layers.[38,39] It should also be noted that the graphene sheet is being kept rigid throughout the simulations to avoid the corrugated nanochannel. The non-bond interactions between carbon and oxygen atoms are

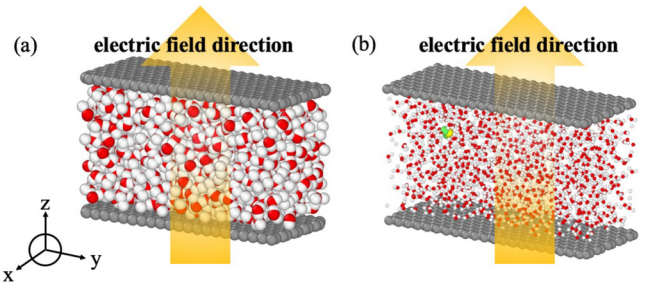

FIG. 1. (a) An example model setup for molecular simulations, where the electric field is applied along the positive z-direction. (b) An example simulation setup for free energy calculations, where a water molecule gradually "disappears" from the simulation domain by gradually switching off its inter-molecular interactions with other molecules. One water molecule (colored in yellow and green) is rendered larger in contrast to other water molecules for visualization purposes.

simulated using the Lennard-Jones (L-J) potential: $E = 4\varepsilon\left[\left(\frac{\sigma}{r_{ij}}\right)^{12} - \left(\frac{\sigma}{r_{ij}}\right)^{6}\right]$, where ε and σ are the energy and length constants, respectively, and r_{ij} is the distance between two atoms I and j. The L-J interactions involving hydrogen atoms are neglected, which is a common practice due to the lightweight of hydrogen atoms.[34] All L-J parameters adopted in the simulations are shown in Table I. A cutoff of 10 Å is chosen for L-J interactions. The long-range electrostatic interaction in the system is computed by the particle-particle particle-mesh (PPPM) approach with an accuracy of 1×10^{-5}. Simulations are performed using the large-scale atomic/molecular massively parallel simulator (LAMMPS).[40] The chosen time step size is 1 fs.

First, the system is energy-minimized and equilibrated in a canonical ensemble (NVT) at 300 K for 5 ns. Then, the system is optimized in an isothermal-isobaric ensemble (NPT) at 1 atm and 300 K for another 2 ns. It should be noted that since each graphene sheet is kept rigid, the graphene surface is flat. However, the spacing between these two rigid graphene sheets is not fixed, and thus, the confined liquid volume can fluctuate and is optimized during the equilibration simulation stage (NPT). 1 atm is being applied to all three directions for our system. Since we used a barostat to control the pressure in each direction independently in the NPT simulation, all directions should have 1 atm pressure. After the structures are fully relaxed, an electric field is applied in the positive z-direction, and the NVE ensemble is then applied to the simulation, which lasts for 2 ns, with the last 1 ns chosen as the

TABLE I. L–J potential ε and σ parameters between graphene and water. "C" represents the carbon atom in the graphene, and "O" represents the oxygen atom in the water molecule.

Pair type	C–O	O–O
$\boldsymbol{\varepsilon}$, $\boldsymbol{ev}$	0.004 06	0.006 73
$\boldsymbol{\sigma}$, Å	3.190	3.166

production period to collect the data. We calculate the water free energy difference between the vacuum state and the state inside the nanochannel using the free energy perturbation method.[41] In such a calculation, one water molecule "gradually disappears" from the nanochannel filled with water by means of a coupling parameter λ that tunes the inter-molecular interaction between the "disappearing" water molecule and the rest of atoms in the system. The interactions tuned include both the L-J interaction and the electrostatic interaction. At $\lambda = 1$, the selected water molecule fully interacts with the rest molecules. At $\lambda = 0$, the selected water molecule is present in the simulation box but does not interact with other molecules. The values between $\lambda = 1$ and 0 are sampled in 200 equal-spaced intervals. We have also sampled 1000 and 500 intervals but found that 200 intervals are sufficient to result in converged results. At each value of λ, the system is equilibrated in the NPT ensemble for 10 ps before free energy calculation. As a result, the calculated free energy is the Gibbs free energy. To avoid the singularities when the selected water molecule decouples with other molecules, soft-cored potentials are used. The free energy difference (ΔG_{1-0}) was calculated using the following equation:

$$\Delta G_{1-0} = -k_B T \sum_{i=1}^{i=0} \ln \left\langle \exp\left(-\frac{U_{\lambda_{i+1}} - U_{\lambda_i}}{kT} \right) \right\rangle, \qquad (1)$$

where k_B is the Boltzmann constant, T is the temperature (300 K in our simulation), and $U_{\lambda_{i+1}} - U_{\lambda i}$ is the pair potential energy difference between each successive perturbation. It should be noted that since the final state ("0") of the "disappearing" water molecules is non-interacting, it is effective in a vacuum. Therefore, a positive value of ΔG_{1-0} means taking water out of liquid requires external energy, i.e., water in liquid is more energetically favorable than in vacuum. Since all calculations used this vacuum level as a reference, a direct comparison of the calculated free energy difference values from different cases will allow us to evaluate the relative thermodynamic stability of water in these cases.

RESULTS AND DISCUSSION

The free energy difference is computed at different external electric field strengths ranging from 0.1 to 0.5 V/Å for the water confined between two graphene layers. We note that these field strengths are high but can be potentially achieved using plasmon-induced local electric fields. For example, it is estimated that the graphene plasmon-induced local electric field is of 10^7–10^8 V/m (10^{-3}–10^{-2} V/Å),[42–47] but for graphene nanopetals functionalized with plasmonic nanoparticles, the field enhancements associated with dipolar plasmons in these spherical nanoparticles can enhance the local field by three orders of magnitude to 1–10 V/Å.[48,49] The influence of the electric field on the free energy difference of the nanoconfined water can be seen in Fig. 2(a). The horizontal red dashed baseline indicates the free energy difference of bulk water in a non-confined phase without

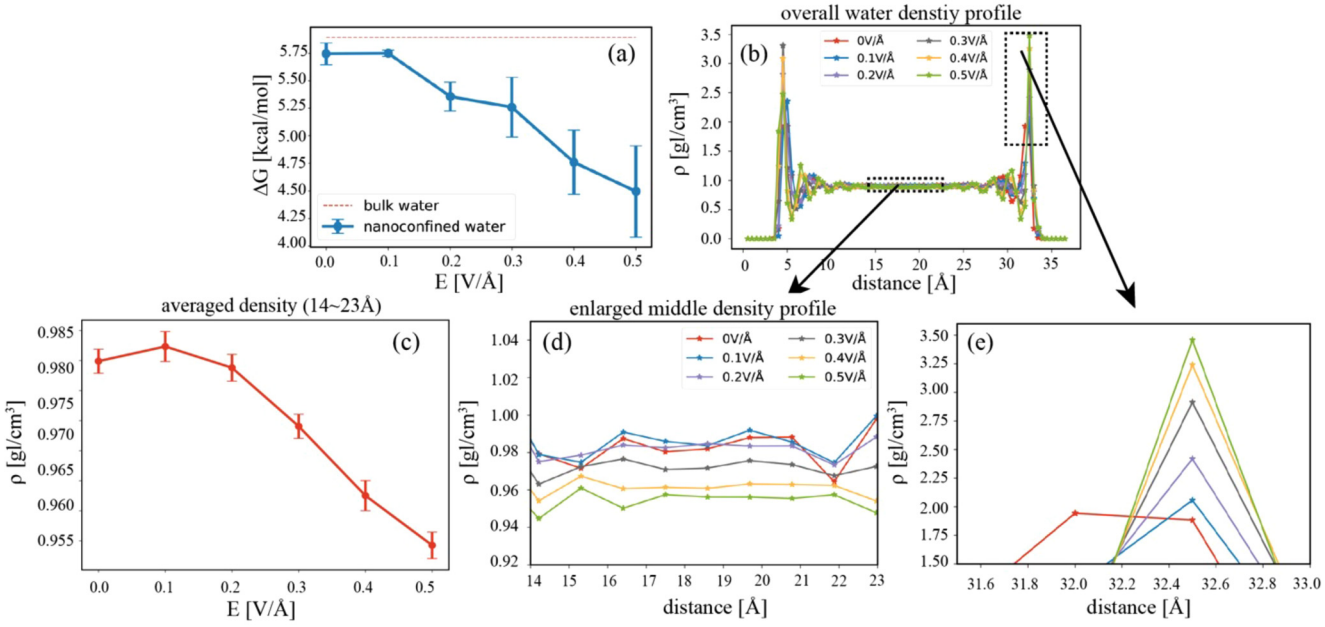

FIG. 2. (a) Water free energy difference (defined as $\Delta G_{1-0} = G_0 - G_1$, where 0 is the reference vacuum state and 1 is the solvated state) in graphene nanochannel under electric fields with different strengths. The error bar is the standard deviation of calculation results from three different perturbation percentage values (1‰, 2.5‰, and 5‰) in the FEP calculations. The horizontal red dashed baseline indicates the free energy difference of water in its bulk phase without an electric field. (b) The water density profile in the graphene nanochannel. (c) The averaged water density of the middle region in the nanochannel under electric fields with different strengths. The error bar is the standard deviation of calculation results from previous mentioned different perturbation percentage values in the FEP calculations. (d) The enlarged water density profile of the middle region from ~14 to 23 Å. (e) A close-up of the electric field-induced water density peaks near the right graphene wall.

the electric field. As we can see, the nanoconfinement lowered water free energy difference with or without an electric field. For the nanoconfined water, the free energy difference shows a systematically decreasing trend as the field strength increases. The results suggest that the nanoconfined environment and the increased field strength make the nanochannel a less thermodynamically favorable environment for water molecules, which potentially makes water evaporation consume less thermal energy, i.e., a reduction in latent heat. However, this does not suggest that water evaporation will cost less energy overall since we have to consider the energy required to transfer bulk water into the nanochannel to overcome the free energy difference between the two states. In addition, the application of an electric field with high strength also requires an energy input (e.g., light-induced plasmonic local field enhancement).

To reveal the mechanism of the electric-field-induced water free energy difference reduction, we further characterized the water structure in the nanochannel by examining the water density under electric fields with different strengths. As shown in Fig. 2(b), due to the presence of graphene, in each case the water profile shows certain structures near the graphene wall that is different from the bulk state as indicated by peaks in the density profile. Figure 2(c) more clearly shows that the averaged water density in the middle portion of the nanochannel decreases with the increasing electric field. The reduced density makes inter-molecular distance larger and, thus, the inter-molecular bonding strength weaker, rendering water less thermodynamically stable in such an environment. The enlarged view of the middle portion (14–23 Å) of the water density profile in Fig. 2(d) shows a decreasing trend as more water molecules are pulled to the graphene interface due to a stronger electric field. As the electric field becomes stronger, more water molecules are being pulled toward the right graphene wall, as shown in Fig. 2(e).

To investigate the influence of the electric field on water spatial distribution, we calculated the radial distribution function between oxygen atoms of water molecules as $g(r) = n(r)/(4\pi r^2 \rho \Delta r)$, where $n(r)$ is the number of atoms in a shell of thickness Δr at a distance r from the reference atom and ρ is the average water atom number density. Figure 3(a) shows the overall water distribution, while Fig. 3(b) clearly shows that as the electric field strength increases, the first nearest-neighbor peak decreases, which indicates that the number of water molecules immediately surrounding each water molecule reduces. The reduced inter-molecular coordination number weakens the inter-molecular interaction and, thus, lowers the free energy difference.

To further understand the molecular-level origin of the electric-field-induced water free energy change, we study the water dipole moment in different directions under different field strengths. The time evolution of the z-component of the total water dipole moment under different field strengths is shown in Fig. 4(a). As expected, it is seen that a larger electric field will lead to larger water polarization in the z-direction, which aligns with the field direction. Since we only applied the electric field in the z-direction, after applying the electric field, only the z-component of the water dipole moment increases noticeably with the increasing external electric field strength as shown in Fig. 4(b), with the dipole moments in the other two directions decreasing slightly. Figures 4(c) and 4(d) showed the snapshots of the molecular system without an external electric field and under an electric field of 0.5 V/Å, respectively. By comparing Figs. 4(c) and 4(d), we can see that most of the positively charged hydrogen atoms in water molecules are being aligned toward the electric field direction as highlighted in the top black box in Fig. 4(d), while most of the negatively charged oxygen atoms in water molecules are being attracted toward the opposite direction of the electric field as highlighted in the bottom black box region. Such observations are also consistent with the foregoing phenomenon that density peak shifts toward the interface between water molecules and graphene walls, which also shows more aligned nanoconfined water molecules.

The alignment of water molecules imposed by the electric field restricts their free rotation, reducing their pecking order, which would, in turn, reduce the intermolecular potential energy.

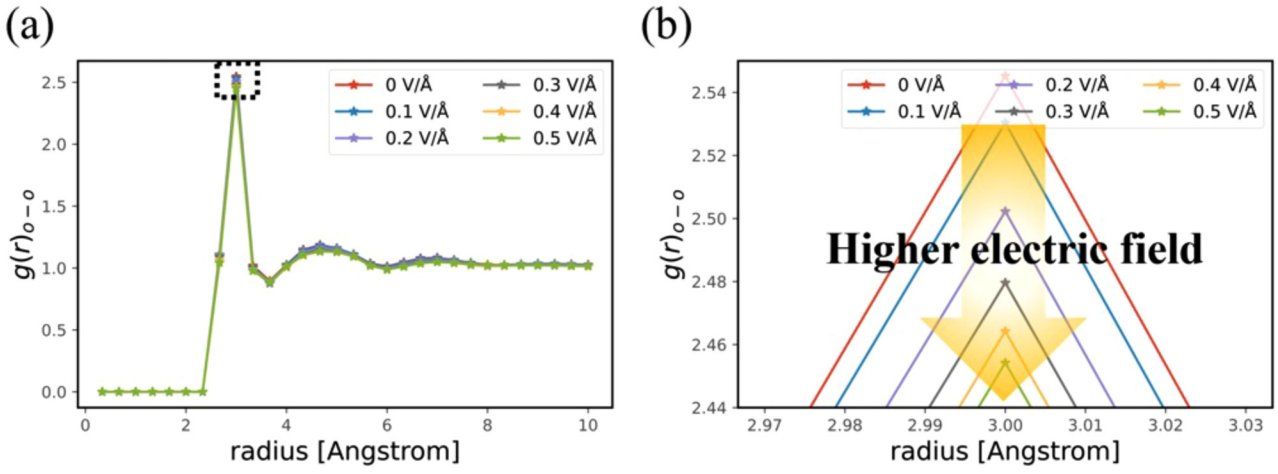

FIG. 3. (a) Radial distribution function (RDF) of the oxygen atoms in water molecules in the nanochannel. (b) A close-up of the black dashed box region in panel.

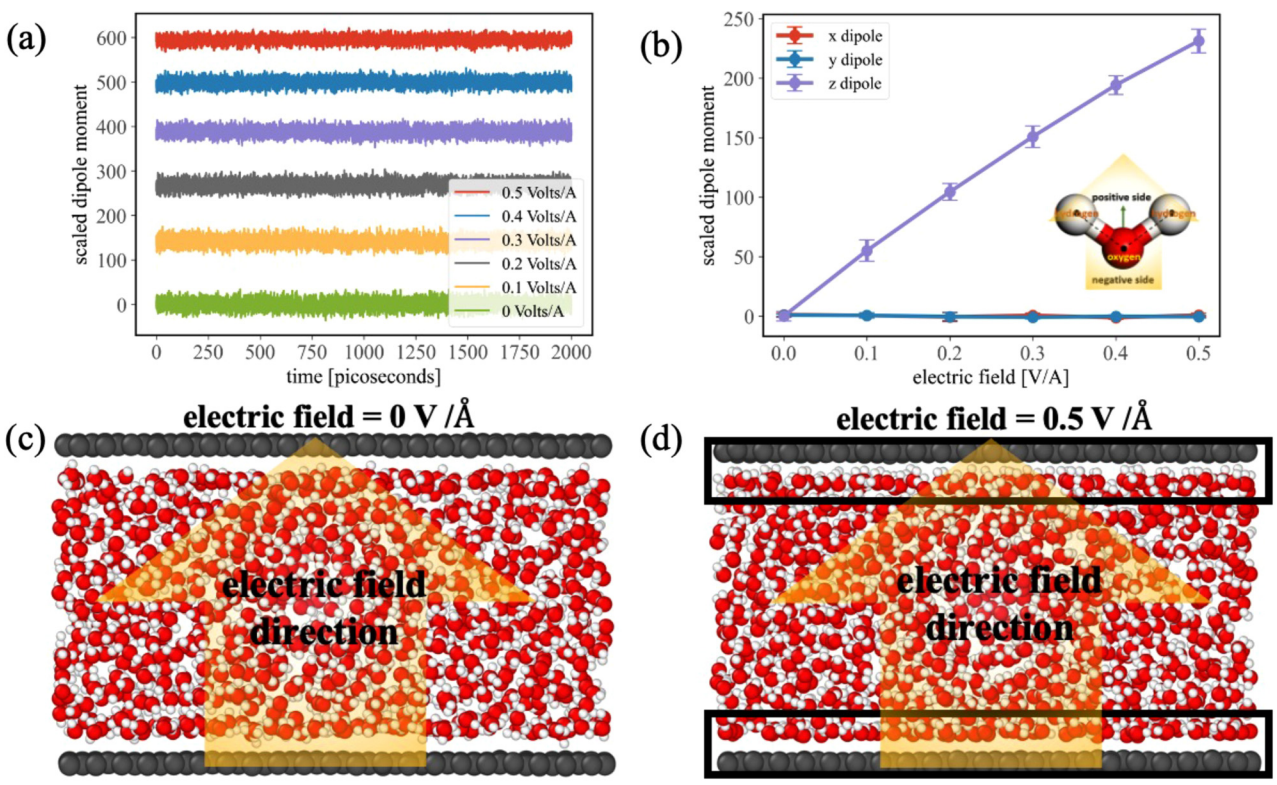

FIG. 4. (a) The z-component of the scaled total water dipole moment evolution under different electric field strengths in the simulation. (b) x-, y-, and z-components of the total scaled water dipole moment under different field strengths. The error bar is the standard deviation of three equilibrated production stages (1 ns) from one single simulation. (c) Snapshot of the equilibrated molecular system when there is no electric field. (d) Snapshot of the equilibrated molecular system under an electric field of 0.5 V/Å.

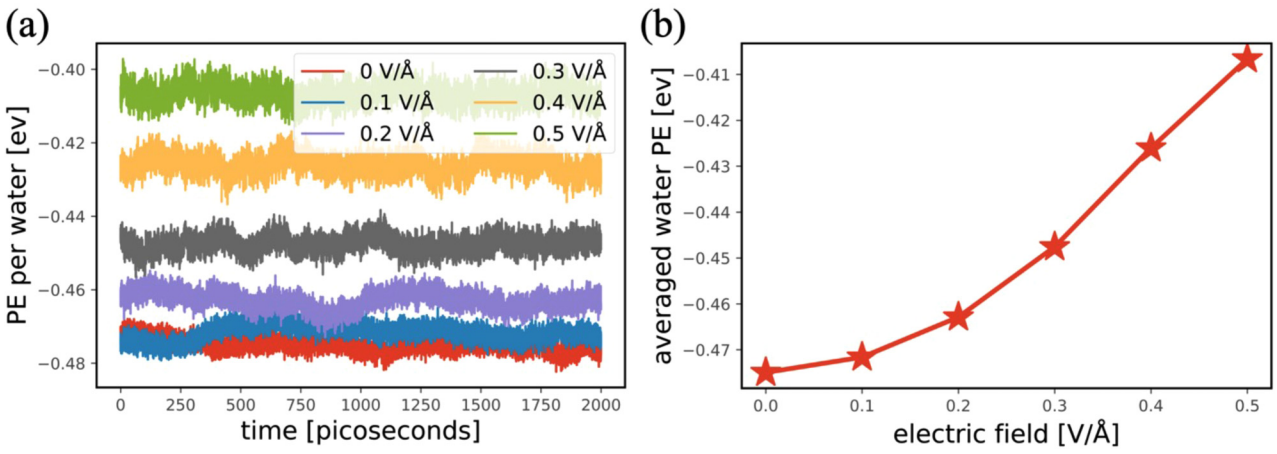

FIG. 5. (a) The potential energy per water molecule as a function of time under different electric fields. (b) The averaged potential energy per water molecule under different electric fields.

We calculate the potential energy per water molecule under different field strengths. Figure 5 shows that as the electric field strength increases, the magnitude of potential energy per water molecule indeed decreases. It should be noted that the calculated potential energy values are negative, which indicate the attraction between each water molecule.

We note that our imposed electric field strengths exceed the dielectric strength of water ($\sim 1 \times 10^7$ V/m), and thus, there could be hydrolysis, which cannot be captured by our currently used fixed bond water model. When hydrolysis happens, part of the electrical energy is devoted to breakdown water. However, it is our belief that the free energy cost in the hydrolysis process will be the same with or without nanoconfinement since this is an individual molecular level process. In addition, we believe that by sweeping the electric field strength in our simulations, the conclusion is general, i.e., electric field in the nanochannel can reduce the water free energy difference. It is just that when the field strength is small, such an effect is expected to be weaker.

CONCLUSION

In summary, we have performed MD simulations to study the Gibbs free energy of water confined in a graphene nanochannel under external electric fields with different strengths. We observe that the free energy difference (defined as $\Delta G_{1-0} = G_0 - G_1$, where 0 is the reference vacuum state and 1 is the solvated state) of water inside the nanochannel is lower than that of water in its bulk phase. We also observe a systematic lowering of this free energy difference of the nanoconfined water with the increasing electric field. The stronger electric field will lead to more aligned water molecules along the electric field direction, which, in turn, lowers the averaged water molecule potential energy. The results from this work show that using an electric field may provide an effective means to reduce the thermal energy required to remove water molecules from nanochannels. We emphasize that our results do not mean water evaporation will consume less energy overall, since we have to consider the energy required to transfer bulk water into the nanochannel to overcome the free energy difference between the two states. In addition, the application of a high electric field also requires energy input (e.g., light-induced plasmonic local field enhancement). However, if the solar-induced plasmonic effect can lead to such high local electric fields via strongly coupled plasmonic hotspots of nanostructures, this part of the energy can be free and renewable, and thermal energy needed can, thus, be reduced, which could be attractive for solar-thermal water evaporation applications.

ACKNOWLEDGMENTS

T.L. and D.H. acknowledge the support from the National Science Foundation (NSF) (Grant No. CBET-1937923), the Center for the Advancement of Science in Space (No. GA-2018-268), and the Dorini Family for the endowed professorship in Energy Studies. G.X. and S.W. acknowledge the University of Texas at Dallas startup fund and the NSF (Grant No. CBET-1937949). The simulations are supported by the Notre Dame Center for Research Computing, NSF through XSEDE computing resources provided by SDSC Comet and Comet and Texas Advanced Computing Center (TACC) Stampede under Grant No. TG-CTS100078, Ganymede HPC Cluster at the University of Texas, and TACC Lonestar5 system.

AUTHOR DECLARATIONS

Conflict of Interest

The authors have no conflicts to disclose.

Author Contributions

Dezhao Huang: Conceptualization (equal); Investigation (equal); Methodology (equal); Software (equal); Validation (equal); Visualization (equal); Writing – original draft (equal); Writing – review and editing (equal). **Shiwen Wu:** Investigation (equal); Writing – original draft (equal); Writing – review and editing (equal). **Guoping Xiong:** Conceptualization (equal); Funding acquisition (equal); Investigation (equal); Project administration (equal); Resources (equal); Supervision (equal); Writing – original draft (equal); Writing – review and editing (equal). **Tengfei Luo:** Conceptualization (equal); Formal analysis (equal); Funding acquisition (equal); Investigation (equal); Methodology (equal); Project administration (equal); Resources (equal); Supervision (equal); Writing – original draft (equal); Writing – review and editing (equal).

DATA AVAILABILITY

The data that support the findings of this study are available from the corresponding authors upon reasonable request.

REFERENCES

[1]M. Nazari, A. Davoodabadi, D. Huang, T. Luo, and H. Ghasemi, Nanoscale **12**, 14626 (2020).
[2]Q. Xie, M. A. Alibakhshi, S. Jiao, Z. Xu, M. Hempel, J. Kong, H. G. Park, and C. Duan, Nat. Nanotechnol. **13**, 238 (2018).
[3]H. Ghasemi, G. Ni, A. M. Marconnet, J. Loomis, S. Yerci, N. Miljkovic, and G. Chen, Nat. Commun. **5**, 4449 (2014).
[4]Y. Ito, Y. Tanabe, J. Han, T. Fujita, K. Tanigaki, and M. Chen, Adv. Mater. **27**, 4302 (2015).
[5]Z. Liu, H. Song, D. Ji, C. Li, A. Cheney, Y. Liu, N. Zhang, X. Zeng, B. Chen, J. Gao, Y. Li, X. Liu, D. Aga, S. Jiang, Z. Yu, and Q. Gan, Glob. Challenges **1**, 1600003 (2017).
[6]P. Zhang, J. Li, L. Lv, Y. Zhao, and L. Qu, ACS Nano **11**, 5087 (2017).
[7]F. Zhao, X. Zhou, Y. Shi, X. Qian, M. Alexander, X. Zhao, S. Mendez, R. Yang, L. Qu, and G. Yu, Nat. Nanotechnol. **13**, 489 (2018).
[8]Y. Pang, J. Zhang, R. Ma, Z. Qu, E. Lee, and T. Luo, ACS Energy Lett. **5**, 437 (2020).
[9]A. W. Knight, N. G. Kalugin, E. Coker, and A. G. Ilgen, Sci. Rep. **9**, 8246 (2019).
[10]D. Muñoz-Santiburcio and D. Marx, Phys. Rev. Lett. **119**, 056002 (2017).
[11]S. H. Garofalini, T. S. Mahadevan, S. Xu, and G. W. Scherer, ChemPhysChem **9**, 1997 (2008).
[12]M. Neek-Amal, F. M. Peeters, I. V. Grigorieva, and A. K. Geim, ACS Nano **10**, 3685 (2016).
[13]N. Giovambattista, P. J. Rossky, and P. G. Debenedetti, J. Phys. Chem. B **113**, 13723 (2009).
[14]N. Giovambattista, P. J. Rossky, and P. G. Debenedetti, Phys. Rev. E **73**, 041604 (2006).
[15]R. Zangi, J. Phys.: Condens. Matter **16**, S5371 (2004).
[16]R. Zangi and A. E. Mark, Phys. Rev. Lett. **91**, 025502 (2003).
[17]J. Gao, W. D. Luedtke, and U. Landman, Phys. Rev. Lett. **79**, 705 (1997).
[18]F. Leoni, C. Calero, and G. Franzese, ACS Nano **15**, 19864 (2021).

[19]L. Figueras and J. Faraudo, Mol. Simul. **38**, 23 (2012).
[20]J. L. Aragones, L. G. MacDowell, J. I. Siepmann, and C. Vega, Phys. Rev. Lett. **107**, 155702 (2011).
[21]Q. Wang, H. Xie, Z. Hu, and C. Liu, Nanomaterials **9**, 64 (2019).
[22]S. Wei, X. Xiaobin, Z. Hong, and X. Chuanxiang, Cryobiology **56**, 93 (2008).
[23]R. Srivastava, J. K. Singh, and P. T. Cummings, J. Phys. Chem. C **116**, 17594 (2012).
[24]K. A. Maerzke and J. I. Siepmann, J. Phys. Chem. B **114**, 4261 (2010).
[25]S.-R. Yeh, M. Seul, and B. I. Shraiman, Nature **386**, 57 (1997).
[26]J. Yang, Y. Pang, W. Huang, S. K. Shaw, J. Schiffbauer, M. A. Pillers, X. Mu, S. Luo, T. Zhang, Y. Huang, G. Li, S. Ptasinska, M. Lieberman, and T. Luo, ACS Nano **11**, 5510 (2017).
[27]W. Xiong, J. Z. Liu, M. Ma, Z. Xu, J. Sheridan, and Q. Zheng, Phys. Rev. E **84**, 056329 (2011).
[28]A. T. Celebi, M. Barisik, and A. Beskok, Microfluid. Nanofluid. **22**, 7 (2018).
[29]O. Neumann, ACS Nano **7**, 42 (2013).
[30]S. Wu, G. Xiong, H. Yang, Y. Tian, B. Gong, H. Wan, Y. Wang, T. S. Fisher, J. Yan, K. Cen, Z. Bo, and K. K. Ostrikov, Matter **1**, 1017 (2019).
[31]B. Gong, H. Yang, S. Wu, G. Xiong, J. Yan, K. Cen, Z. Bo, and K. Ostrikov, Nano-Micro Lett. **11**, 51 (2019).
[32]S. Wu, G. Xiong, H. Yang, B. Gong, Y. Tian, C. Xu, Y. Wang, T. Fisher, J. Yan, K. Cen, T. Luo, X. Tu, Z. Bo, and K. K. Ostrikov, Adv. Energy Mater. **9**, 1901286 (2019).
[33]C. Xu, Z. Bo, S. Wu, Z. Wen, J. Chen, T. Luo, E. Lee, G. Xiong, R. Amal, A. T. S. Wee, J. Yan, K. Cen, T. S. Fisher, and K. K. Ostrikov, Solar Energy **208**, 379 (2020).
[34]D. J. Price and C. L. Brooks, J. Chem. Phys. **121**, 10096 (2004).
[35]A. D. MacKerell, D. Bashford, M. Bellott, R. L. Dunbrack, J. D. Evanseck, M. J. Field, S. Fischer, J. Gao, H. Guo, S. Ha, D. Joseph-McCarthy, L. Kuchnir, K. Kuczera, F. T. Lau, C. Mattos, S. Michnick, T. Ngo, D. T. Nguyen, B. Prodhom, W. E. Reiher, B. Roux, M. Schlenkrich, J. C. Smith, R. Stote, J. Straub, M. Watanabe, J. Wiórkiewicz-Kuczera, D. Yin, and M. Karplus, J. Phys. Chem. B **102**, 3586 (1998).
[36]Z. Futera and N. J. English, J. Chem. Phys. **147**, 031102 (2017).
[37]Y. Hu and G. Jia, Physica A **564**, 125275 (2021).
[38]E. Barani, I. P. Lobzenko, E. A. Korznikova, E. G. Soboleva, S. V. Dmitriev, K. Zhou, and A. M. Marjaneh, Eur. Phys. J. B **90**, 38 (2017).
[39]G. Dhaliwal, P. B. Nair, and C. V. Singh, Carbon **142**, 300 (2019).
[40]S. Plimpton, J. Comput. Phys. **117**, 1 (1995).
[41]R. W. Zwanzig, J. Chem. Phys. **22**, 1420 (1954).
[42]P. F. Liao and A. Wokaun, J. Chem. Phys. **76**, 751 (1982).
[43]J. A. Sánchez-Gil, Phys. Rev. B **68**, 113410 (2003).
[44]P. C. Das and J. I. Gersten, Phys. Rev. B **25**, 6281 (1982).
[45]A. V. Ermushev, B. V. Mchedlishvili, V. A. Oleĭnikov, and A. V. Petukhov, Quantum Electron. **23**, 435 (1993).
[46]J. Jersch, F. Demming, L. J. Hildenhagen, and K. Dickmann, Appl. Phys. A: Mater. Sci. Process. **66**, 29 (1998).
[47]Y. C. Martin, H. F. Hamann, and H. K. Wickramasinghe, J. Appl. Phys. **89**, 5774 (2001).
[48]Y. Wu and P. Nordlander, J. Chem. Phys. **125**, 124708 (2006).
[49]K. Li, M. I. Stockman, and D. J. Bergman, Phys. Rev. Lett. **91**, 227402 (2003).